PAPER

Nonlinear simulations of thermo-resistive tearing mode formalism of the density limit

To cite this article: Q. Teng *et al* 2018 *Nucl. Fusion* **58** 106024

View the article online for updates and enhancements.

Nonlinear simulations of thermo-resistive tearing mode formalism of the density limit

Q. Teng[1], N. Ferraro, D.A. Gates and R.B. White

Princeton Plasma Physics Laboratory, Princeton University, Princeton, NJ, United States of America

E-mail: tengqian0001@gmail.com

CrossMark

Abstract

This work is an extension of the previous semi-analytical work (Teng *et al* 2016 *Nucl. Fusion* **56** 106001), explaining the density limit with a thermo-resistive tearing mode model. The thermo-resistive island growth is calculated with a 3D MHD code M3D-C^1 (Jardin *et al* 2012 *Comput. Sci. Discovery* **5** 014002). It is shown with nonlinear 3D MHD simulations that impurity radiation stimulates large magnetic islands at the density limit. The impact of thermal perturbations inside and outside of the island is explored. Inside the island, net cooling enhances the island growth and net heating suppresses its growth. Outside the island, thermal perturbations have a much smaller impact on the island growth. When the plasma density is increased towards the density limit, the island changes from being heated to being cooled and grows to a much larger island width. The convergence test of the simulations over the temporal and spatial grid is performed. The numerical model and the semi-analytical model are compared by calculating the Δ' terms, which are defined in the modified Rutherford equation, and good agreement is observed.

Keywords: density limit, tearing mode, impurity radiation, MHD simulation

(Some figures may appear in colour only in the online journal)

1. Introduction

In every tokamak, there is a maximum operational plasma density, above which the confinement is unstable and usually is ended with a major disruption [3–6]. Greenwald [7, 8] proposed the most succesful empirical scaling law of the density limit by fitting the density limit dataset of multiple tokamaks,

$$\bar{n}_G(10^{20} \text{ m}^{-3}) = \frac{I_\mathrm{p}(\mathrm{MA})}{\pi a^2(\mathrm{m}^2)}, \qquad (1)$$

where $\bar{n}_G$ is the line-averaged plasma density, I_p is the plasma current and πa^2 is the plasma cross section area. Understanding the physical mechanism of the density limit is a crucial task. The disruptions in density limit discharges can cause major damages to the plasma facing components of tokamaks. It is important to understand and exceed the density limit as the fusion power is proportional to the square of plasma density. Much efforts has been devoted to explaining this robust phenomenon. Many theories try to explain the density

limit based on the accompanying phenomenology, such as MARFEs, diverter detachment, poloidal detachment, the H-L transition, current channel shrinkage and MHD instabilities [4, 9–13]. But none of them can explain the density limit quantitatively and with the correct phenomenology. Experiments show that the density limit is associated with cooling of the edge plasma and radiation and the density limit can be exceeded by increasing the core plasma density [14–18]. In the previous semi-analytical work [1], we proposed a thermo-resistive model that predicts the density limit quantitatively correct and with the right phenomenology. When the plasma density is increased toward the density limit, the current profile becomes more peaked, reducing local Ohmic heating inside the island, and the impurity radiation is increased. The island changes from being heated and suppressed to being cooled and stimulated. When the plasma density reaches the density limit, the island grows so large that it can lead to loss of confinement. In this work, we calculate the thermo-resistive tearing mode growth approaching the density limit with a 3D MHD code.

The rest of the paper is structure as follows. Section 2 presents the numerical methods. Section 3 describes the

---

[1] Author to whom any correspondence should be addressed.

equilibrium used in simulations. Sections 4 and 5 present the numerical results of the thermo-resistive tearing modes and the density limit. Section 6 compares the numerical results withe semi-analytical calculations. Section 7 gives a summary of the conclusions. The convergence test of the simulations is presented in the appendix.

2. Numerical methods

The M3D-C^1 code is a scalable fully implicit time advance finite element code that solves a set of visco-resistive two-fluid equations [19]. This work aims to explain the density limit with a thermo-resistive tearing mode model, thus requiring accurate calculation of the tearing mode growth and heat transport. The viscous terms, two-fluid terms and gyro-viscosity terms are not considered here. A resistive MHD model is used,

$$\frac{\partial \rho}{\partial t} + \nabla \cdot (\rho \vec{V}) = 0, \tag{2}$$

$$\rho \frac{d\vec{V}}{dt} = \vec{j} \times \vec{B} - \nabla p, \tag{3}$$

$$\frac{3}{2}\frac{\partial p}{\partial t} + \nabla \cdot \left(\frac{3}{2}p\vec{V}\right) = -p\nabla \cdot \vec{V} + \eta j^2 - P_{\text{rad}}$$
$$+ \nabla \cdot \left[\chi_\perp \nabla_\perp p + \chi_\parallel \nabla_\parallel p\right] - \Pi : \nabla\vec{V}, \tag{4}$$

$$\frac{\partial \vec{B}}{\partial t} = -\nabla \times \vec{E}, \tag{5}$$

$$\eta \vec{j} = \vec{E} + \vec{V} \times \vec{B}, \tag{6}$$

$$\mu_0 \vec{j} = \nabla \times \vec{B}, \tag{7}$$

$$\nabla \cdot \vec{B} = 0, \tag{8}$$

where $\chi_\perp$ and $\chi_\parallel$ are the perpendicular and parallel heat diffusivity respectively, Π is the viscosity tensor. Plasma is cooled through Bremsstrahlung continuum radiation as well as impurity line radiation. The radiation power is calculated by $P_{\text{rad}} = \sum_Z n_e n_Z L_Z(T_e)$, where $L_Z(T_e)$ is the cooling rate calculated from the model presented in [20]. The tearing mode evolution spans the resistive time $\tau_R = \mu_0 L^2/\eta$ and the Alfven time $\tau_A = \sqrt{\mu_0 \rho}L/B$. In the typical fusion plasma regime, the Lundquist number $S = \tau_R/\tau_A \sim 10^7$ at the plasma edge. The large time scale separation is one of the biggest challenges to resistive MHD simulations. The extremely high anisotropy is another challenge, and the heat conduction along the magnetic field lines, dominated by free-streaming electrons, is much faster than the cross-field transport, mainly driven by the turbulence. The parallel heat transport coefficient is estimated to be around 10^8 times the perpendicular heat transport coefficient. It is essential to calculate the heat diffusion equation accurately to model the thermal effects on the island growth. An inaccurate diffusion model could drastically underestimate or overestimate the thermal effects.

In order to solve these challenges, M3D-C^1 uses a scalable fully implicit time advance method to avoid the Courant condition set by MHD wave velocities or plasma flow. But the implicit matrix equation is still highly ill conditioned due to the large time scale separation and the high anisotropy. Multiple techniques have been implemented to improve the effective condition number of the matrix, including the split implicit method, annihilation operators and the block-Jacobi preconditioner. The split implicit method represents new time pressure and magnetic field variables with new time velocity variables. Solving one time step is changed from solving a large anti-symmetric matrix equation with large off-diagonal elements to solving a smaller diagonally dominant symmetric matrix equation. The new time pressure and magnetic field variables are then calculated with new time velocity solutions explicitly. The annihilation operators transform the ill conditioned matrix equation into a matrix with three approximately diagonal blocks each multiplied with a separate component of the velocity field. The condition numbers of the three sub-matrices are much smaller than the original single large matrix. The block-Jacobi preconditioner is applied due to the strong coupling within a plane and the highly anisotropic heat diffusivity. By inverting the components within the poloidal planes simultaneously, the condition number is greatly reduced. These techniques enable M3D-C^1 to solve the resistive MHD equations efficiently and calculate the anisotropic heat diffusion process accurately.

3. The self-consistent Furth–Rutherford–Selberg equilibrium

A right-handed (r, θ, ϕ) cylindrical coordinate is used in the simulations and the equilibrium is assumed to be symmetric in the θ and ϕ direction. The equilibrium fluid velocity $\vec{V}$ is 0. The plasma density and toroidal electricity field strength are constant and uniform. The equilibrium profiles are solutions of the steady state resistive MHD equations together with the Spitzer resistivity model,

$$\vec{j} \times \vec{B} - \nabla p = 0, \tag{9}$$

$$\frac{1}{r}\frac{d}{dr}\left(r\chi_\perp \frac{dp}{dr}\right) + \eta j^2 = 0, \tag{10}$$

$$\eta \vec{j} = \vec{E}, \tag{11}$$

$$\eta = \frac{\pi Z e^2 \sqrt{m_e} ln\Lambda}{(4\pi\epsilon)^2 (k_B T)^{3/2}}. \tag{12}$$

The impurity radiation term is very small and ignored when calculating the initial equilibrium. The self-consistent FRS equilibrium resembles the equilibrium observed in tokamaks. The toroidal current density profile is,

$$j(r) = j_0 \left[1 + \left(\frac{r}{r_0}\right)^{2\nu}\right]^{-(1+1/\nu)}, \tag{13}$$
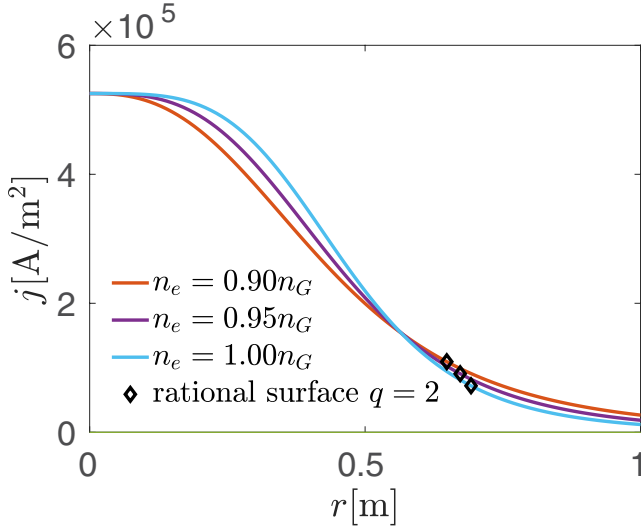
Figure 1. Equilibrium current density profiles with different plasma densities.
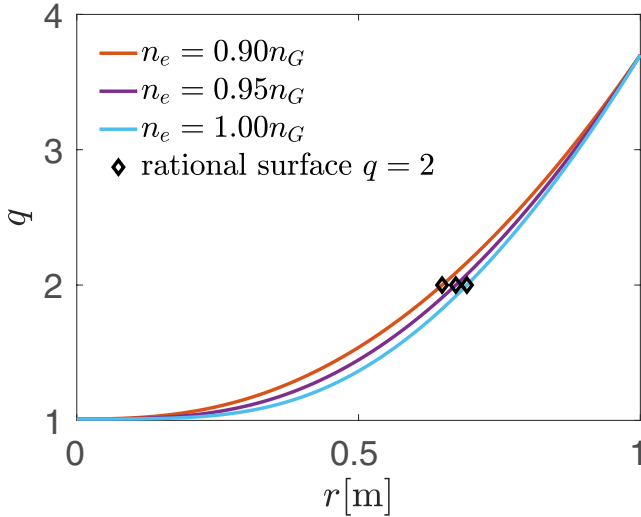

Figure 2. Equilibrium safety factor profiles with different plasma densities.

where j_0 is current density on the axis, r_0 is the width of current channel, ν is the peaking factor of the current density profile. Figure 1 plots typical equilibrium current density profiles. The safety factor profile is,

$$q(r) = q_0 \left[1 + \left(\frac{r}{r_0} \right)^{2\nu} \right]^{1/\nu}, \tag{14}$$

where q_0 is the safety factor on the axis. Figure 2 plots typical equilibrium safety factor profiles. As a result, the pressure profile is,

$$p(r) = p_0 \left[1 + \left(\frac{r}{r_0} \right)^{2\nu} \right]^{-\frac{2}{3}(1+1/\nu)}. \tag{15}$$

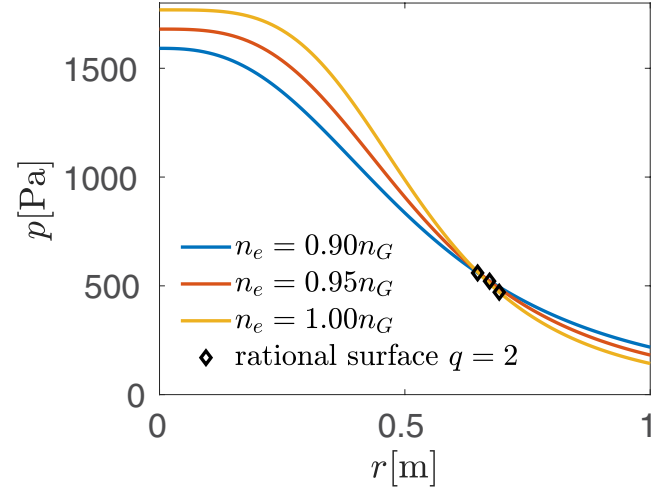Figure 3 plots typical equilibrium pressure profiles. The perpendicular heat diffusivity profile is,

Figure 3. Equilibrium pressure profiles with different plasma densities.
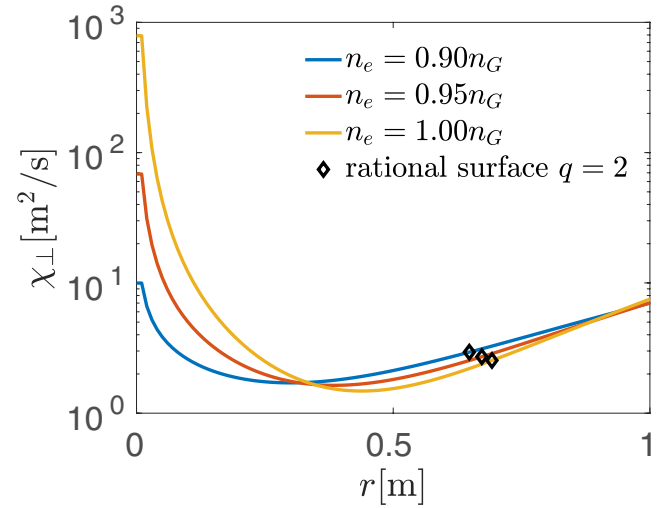

Figure 4. Equilibrium perpendicular heat diffusivity profiles with different plasma densities.

$$\chi_\perp(r) = \frac{3Ej_0 r_0^2}{8(1+\nu)p_0} \left(\frac{r}{r_0} \right)^{2-2\nu} \left[1 + \left(\frac{r}{r_0} \right)^{2\nu} \right]^{\frac{5}{3}-1/3\nu}. \tag{16}$$

Figure 4 plots typical equilibrium perpendicular heat diffusivity profiles. The perpendicular heat diffusivity profile is singular on axis because the pressure profile is completely flat on the axis. Although this is not consistent with the experiments, the thermo-resistive tearing mode model is insensitive to the shape of equilibrium profiles in the center. The toroidal magnetic field is determined by,

$$\frac{\mathrm{d}B_\phi}{\mathrm{d}r}$$

$$= \frac{\mu_0 p_0 \frac{8}{3}(1+\nu) \left[1 + \left(\frac{r}{r_0} \right)^{2\nu} \right]^{-\frac{5}{3}-\frac{2}{3\nu}} \left(\frac{r}{r_0} \right)^{2\nu-2} \frac{r}{r_0^2} - \frac{4B_\phi^2}{R^2 q^2} r \left[1 + \left(\frac{r}{r_0} \right)^{2\nu} \right]^{-1}}{2B_\phi \left(1 + \frac{r^2}{R^2 q^2} \right)}. \tag{17}$$

As a low beta equilibrium is used, the toroidal magnetic field B_ϕ varies by only a few percent from the axis to the edge
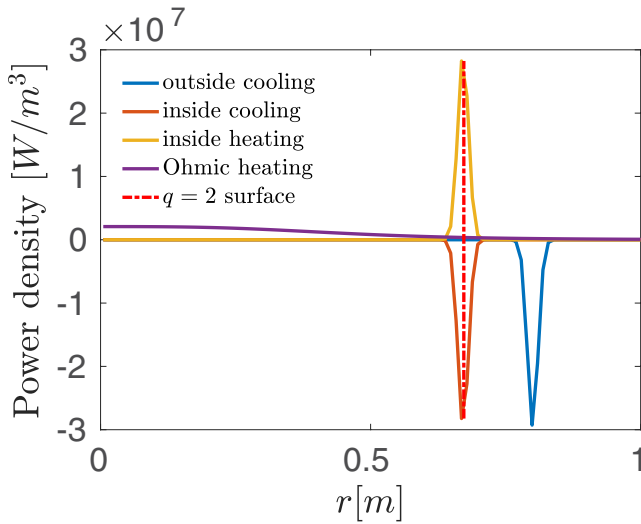
Figure 5. Heat sources located at different radii.

Figure 6. Island growth under different perturbations.

in simulations and can be considered uniform. The self-consistent FRS equilibrium enables direct comparison to the semi-analytic model though there are some minor differences between the equilibrium used in the two models. In the simulation, the initial equilibrium is provided by the self-consistent FRS equilibrium. A perfectly conducting wall at the plasma boundary is used at the boundary condition.

4. Impacts of thermal perturbations on the tearing mode growth

Although the resistive MHD equations are solved in the simulations, it is a useful and intuitive to analyze the modified Rutherford Equation to understand the different terms that contribute to the island evolution [21, 22].

$$\frac{\mathrm{d}w}{\mathrm{d}t} = 1.66 \frac{\eta}{\mu_0} \left[\Delta'_{\mathrm{ql}}(w) + \Delta'_{\mathrm{A}}(w) + \Delta'_{\delta j}(w) \right]. \qquad (18)$$

As shown by the equation, thermal perturbations affect the island growth in two ways. Firstly, thermal perturbations change the global current density profile, thus modifying the Δ'_{ql} term. Secondly, thermal perturbations change the temperature and current density profile inside the island, thus modifying the $\Delta'_{\delta j}$ term. It will be shown numerically later in figure 6 that for the same amount of thermal perturbation, the second effect is much more effective in changing the island growth.

A Gaussian heat source is introduced to explore the thermal effects on the island growth. The heat source is centered at a spot on the poloidal plane with a Gaussian distribution. As the heat source is symmetric in the ϕ direction and the heat is equilibrated quickly along the magnetic field lines, it effectively heats a band area that extends poloidally from the spot. Gaussian heat sources with the same absolute value centered at the $q = 2$ surface and outside the island are used in the simulations. Figure 5 plots the power densities of heating and cooling sources centered at different radii and the Ohmic heating power for comparison. The island width evolution
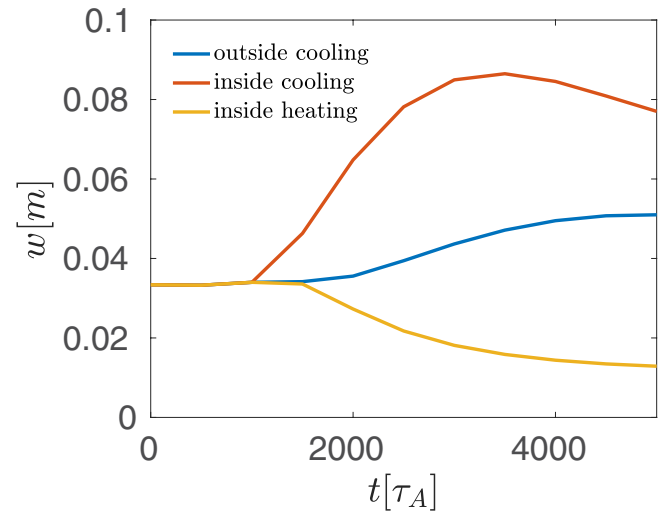
is plotted in figure 6. In this simulation, the island saturates at 0.034 m when there is no external thermal perturbation. The Gaussian heat sources are introduced after the island has reached saturation. The island grows to 0.086 m when there is net cooling inside the island. The island shrinks to 0.012 m when there is net heating inside the island. The island grows to 0.051 m when there is net cooling outside the island. Net cooling/heating inside the island greatly increases/reduces the maximum island width. The island growth is less sensitive to thermal perturbations outside the island. This is consistent with experiment observations that electron cyclotron resonance heating reduces the island width significantly [23–25].

5. Significant growth of the tearing mode at the density limit

The equilibrium changes as the plasma density is increased in experiments. This work does not aim to study how the equilibrium evolves but uses a systematic method to set the initial FRS equilibrium in each simulation as a function of the plasma density as an approximation to the experiments. In density limit discharge experiments, q_0 and q_{edge} are roughly constant as the plasma density is increased and thus are assumed to be fixed in the simulation. The normalized internal inductance l_{i} is observed to increase and reach a maximum value when the plasma density is increased towards the density limit [26]. An ad hoc model is used to describe the l_{i} dependence on n_e,

$$l_{\mathrm{i}}(n_e) = \begin{cases} (l_{\mathrm{i,max}} - l_{\mathrm{i,min}}) \frac{\bar{n}_e/\bar{n}_{\mathrm{G}} - 0.7}{0.3} + l_{\mathrm{i,min}} & \text{if } \bar{n}_e/\bar{n}_{\mathrm{G}} > 0.7 \\ l_{\mathrm{i,min}} & \text{if } \bar{n}_e/\bar{n}_{\mathrm{G}} \leqslant 0.7 \end{cases} \qquad (19)$$
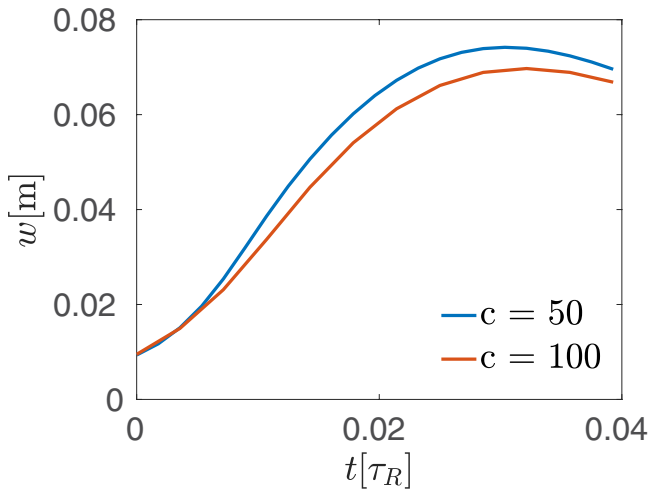
where,

$$l_{\mathrm{i,max}} = (0.12 q_{\mathrm{edge}} \cdot h + 0.6) \cdot h, \qquad (20)$$

$$l_{\mathrm{i,min}} = (-0.08 q_{\mathrm{edge}} \cdot h + 1.05) \cdot h, \qquad (21)$$

where $h = (1 + \kappa^2)/(2\kappa)$ approximates the modifications of l_{i} and q_{edge} due to elongation κ. For a chosen plasma density, l_{i} is calculated from the ad hoc model. The other FRS equilibrium

Table 1. Experimentally relevant parameters.

R	a	q_0	q_{edge}	B_ϕ	U	$n_{Fe}(r_s)/n_e(r_s)$	$\chi_\perp$	$\chi_\parallel/\chi_\perp$
3 m	1 m	1.01	3.7	1 T	1 V	1.5×10^{-4}	$\sim$2.4 m^2 s^{-1}	10^8

Figure 7. Island growth with different scaling parameter.

Figure 8. Change of tearing mode evolution as the plasma density approaches the density limit in the numerical model.

parameters are calculated from the chosen q_0, q_{edge} and the l_i. Simulation parameters are chosen to be representative for discharges at the density limit in typical tokamaks. In table 1, R is the major radius, a is the minor radius, and U is the loop voltage. Only Iron is included to represent the impurities because the impurity radiation is usually dominated by high Z impurities. The iron density is $1.5 \times 10^{-4} n_e$ between $r_s - \delta$ and $r_s + \delta$ and 0 elsewhere, where r_s is the $q = 2$ surface and $\delta = 0.1$ m. This impurity density profile minimizes its impact on the equilibrium profiles. As the tearing mode growth spans the Alfven time and the resistive time, the number of time steps it takes for the island to saturate is roughly proportional to the Lundquist number S. $S \approx 10^7$ for these parameters and it takes too long for the tearing mode to grow and saturate. We propose a method to keep the thermo-resistive island growth almost the same while reducing S and required number of time steps significantly. η, U, $\chi_\parallel$, $\chi_\perp$, and n_{Fe} are scaled by the same factor,

$$\eta,\ U,\ \chi_\parallel,\ \chi_\perp, n_{Fe} \to c\eta,\ cU,\ c\chi_\parallel,\ c\chi_\perp, cn_{Fe}. \quad (22)$$

The other parameters are kept the same. The steady state resistive MHD equations are transformed to,
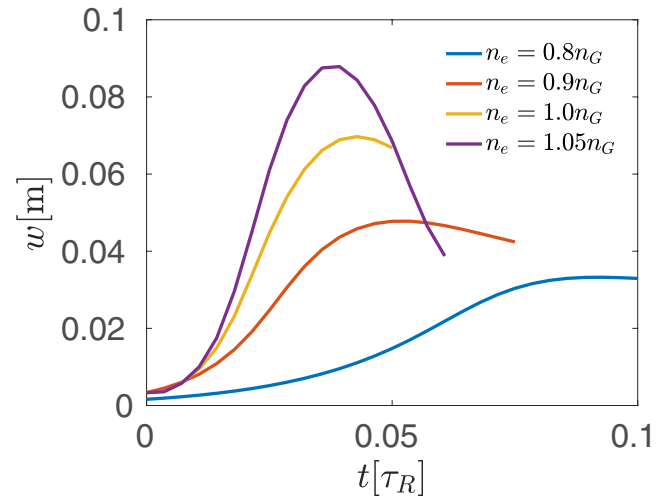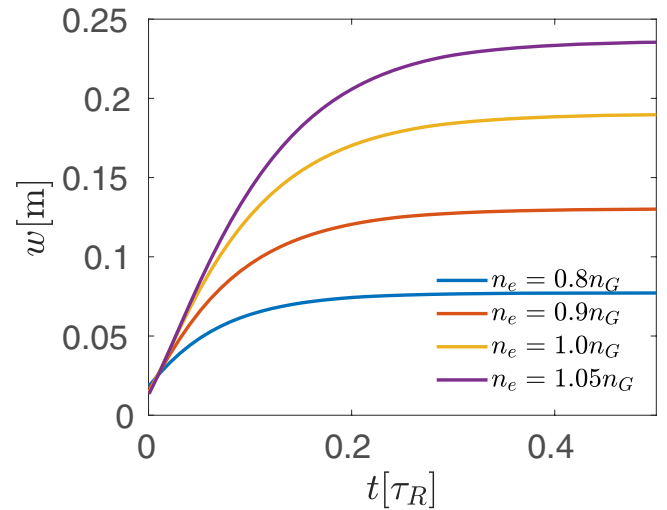
$$\vec{j} \times \vec{B} - \nabla p = 0, \quad (23)$$

$$\frac{1}{r}\frac{\mathrm{d}}{\mathrm{d}r}\left(rc\chi_\perp\frac{\mathrm{d}p}{\mathrm{d}r}\right) + c\eta j^2 = 0, \quad (24)$$

$$c\eta\vec{j} = c\vec{E}. \quad (25)$$

The scaling factor c is cancelled on both sides and the equilibrium remains the same. The thermal perturbation is solved from the diffusion equation,

$$0 = \nabla \cdot (c\chi_\perp\nabla_\perp p + c\chi_\parallel\nabla_\parallel p) + c\eta j^2 - cP_{rad}. \quad (26)$$

The scaling factor c is cancelled on both sides and the temperature perturbation δT and current perturbation δj remain the

Figure 9. Change of tearing mode evolution as the plasma density approaches the density limit in the semi-analytical model.

same. As $\Delta'_{\delta j} \propto \langle \delta j \rangle$, the impact of impurity radiation on the island growth remains the same under this transformation. The Lundquist number is transformed to,

$$S = \frac{\tau_R}{\tau_A} = \frac{\sqrt{\mu_0}LB}{c\eta\sqrt{\rho}}. \quad (27)$$

S is scaled by $1/c$ and the required simulation time steps and the CPU hours are reduced by $1/c$. Figure 7 plots the island growth with the scaling factor $c = 50$ and $c = 100$. The island growth deviates by only a few percent when the scaling factor is different by a factor of 2, showing that the scaling method does not change thermal effects on the island growth.

A series of simulations are performed to calculate the island growth at different plasma densities, see figure 8. Using scaling
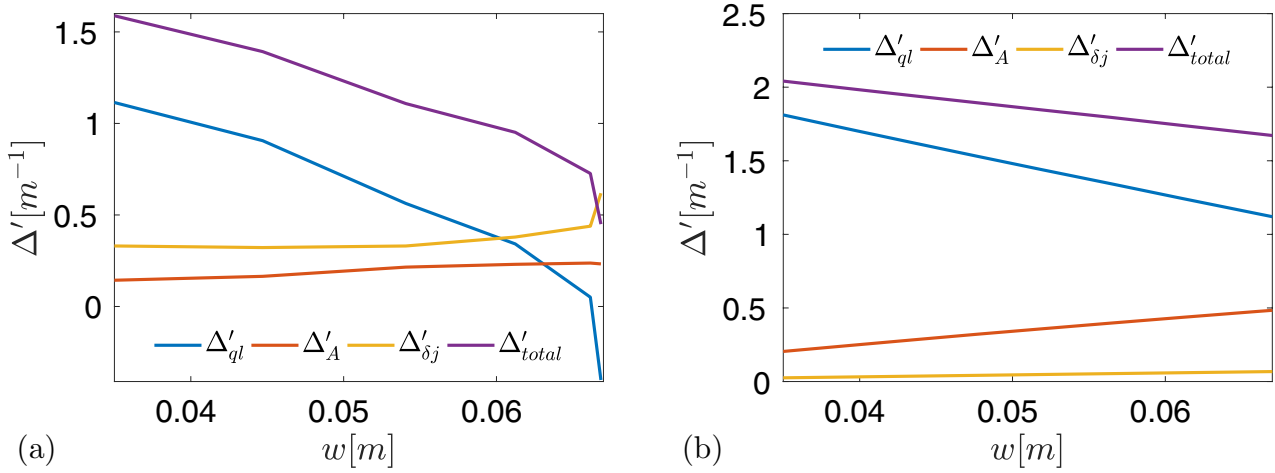
Figure 10. Δ' terms in the numerical model and the semi-analytical model. (*a*) Δ' terms in numerical model. (*b*) Δ' terms in semi-analytical model.

factor $c = 100$, each simulation takes around 6000 CPU hours. In each simulation, the island grows and saturates at a certain size then shrinks to a smaller size. Comparing different simulations, the island grows to a much larger size when the plasma density is increased toward the density limit. The maximum island width increases by about 170% from 0.033 m to 0.088 m as n_e is increased from $0.8n_G$ to $1.05n_G$. When the plasma density is increased, the impurity radiation power increases proportionally, and the Ohmic heating power decreases due to the more peaked current density profile. The thermal perturbation of the island changes from net heating to net cooling and the island grows to a larger size. As a comparison, the island growth is also calculated with the semi-analytical model using the same parameters, see figure 9. The island grows and saturates at certain size because unlike the numerical calculations the equilibrium is assumed to be fixed in the semi-analytical model. The maximum island width increases by about 200% from 0.078 m to 0.237 m as n_e is increased from $0.8n_G$ to $1.05n_G$.

Though the numerical simulations show that the magnetic island grows to a larger size when approaching the density limit, the numerical model still underestimates the thermo-resistive effects on the magnetic island growth in two ways. Firstly, the anisotropy of heat diffusivity $\chi_\parallel/\chi_\perp = 10^8$ in the simulations but this value might be even larger in experiments. The critical island width w_f is proportional to $(\chi_\parallel/\chi_\perp)^{-1/4}$, thus the w_f used in simulations is about larger typical values in experiments. $\Delta_{\delta j}$, which is proportional to $w^2/(w^2 + w_f^2)$, is underestimated. Secondly, the perpendicular heat diffusivity inside the island $\chi_\perp$ is about 10% of the value outside the island in experiments [27, 28]. But the numerical model assumes $\chi_\perp$ outside and inside the island to be the same. Properly including this effect will increase the thermo-resistive impact further.

6. Comparison of the numerical model and the semi-analytical model

The numerical model and the semi-analytical model are similar in many ways. Both model use similar equilibrium profiles and the same equilibrium evolution model as the plasma

density is increased. Both model use same parameters in the calculation, except that the numerical model scales the parameters by 100. But there are also some important differences between the two models that lead to the differences in their results. The numerical model solves the three-dimensional resistive MHD equations and allow the equilibrium to change as the tearing mode grows. The semi-analytical model solves the modified Rutherford equation, which is a simplification of the resistive MHD model, and assumes the equilibrium to be fixed as the tearing mode grows.

The tearing mode growth in the numerical model and the semi-analytical model are compared directly by calculating the Δ' terms defined by the modified Rutherford equation (18). The Δ' terms are defined as,

$$\Delta'_{\mathrm{ql}} = \psi'_1\big|_{r_1}^{r_r} / \psi_1(r_s), \tag{28}$$

$$\Delta'_A = -\frac{2\pi R\mu_0}{\psi_1(r_s)} f_F \frac{m}{\pi} \int_{-\pi/m}^{\pi/m} \mathrm{d}\theta \int_{\tilde{r}_1(\theta)}^{\tilde{r}_r(\theta)} \mathrm{d}r(j_0(r_x) - j_0(r)) \cos(m\theta), \tag{29}$$

$$\Delta'_{\delta j} = -\frac{2\pi R\mu_0}{\psi_1(r_s)} f_F \frac{m}{\pi} \int_{-\pi/m}^{\pi/m} \mathrm{d}\theta \int_{\tilde{r}_1(\theta)}^{\tilde{r}_r(\theta)} \mathrm{d}r(j(r) - j_0(r_x)) \cos(m\theta) \tag{30}$$

where R is the major radius, ψ_1 is the first harmonic of the perturbed helical flux, f_F is the flattening factor of order unity, r_1 is the left edge of the island, r_r is the right edge of the island, $\tilde{r}_1$ is the left half of the separatrix, $\tilde{r}_r$ is the right half of the separatrix. Δ'_{ql} is the discontinuity of the perturbed helical flux across the island. Δ'_A is the integrated current perturbation caused by the flattening of the current density profile by the asymmetric island. $\Delta'_{\delta j}$ is the integrated current perturbation caused by excessive heating or cooling of the island. Although M3D-C^1 does not solve the modified Rutherford equation, the Δ' terms defined above can still by calculated numerically and compared against the semi-analytical model. Figure 10 shows an example of the Δ' terms by the numerical model and semi-analytical model of a tearing mode under net cooling using the same

parameters. The Δ' terms in both models have similar trends and values. Δ'_{total} terms are initially positive and decreases to zero as the island grows and saturates. Δ'_{ql} decreases monotonically as the island grows. Δ'_A and $\Delta'_{\delta j}$ increase weakly as the island grows. Δ'_A and Δ'_{ql} in the numerical and semi-analytical calculations agrees well in magnitude. The $\Delta'_{\delta j}$ term is much larger in the numerical calculation, because M3D-C^1 solves the heat diffusion equation and the thermal perturbation term is modeled better. The numerical model and the semi-analytical model are similar, and their results can be compared against each other.

7. Summary

A numerical model is developed to simulate the thermo-resistive tearing mode growth when the plasma density is increased toward the density limit. The numerical model is an improvement of the semi-analytical model. An advanced finite element code M3D-C^1 is used to solve the resistive MHD equations. The large time scale separation and high anisotropy problem is solved by using the split implicit method, annihilation operators and the block-Jacobi preconditioner. A pressure gradient dependent thermal diffusivity model is implemented as an attempt to include the reduced diffusivity inside the island, though it turns out to be numerically unstable. A scaling method is developed and the CPU hour is reduced greatly. The self-consistent FRS equilibrium is used in the simulations. The convergence of the simulations is examined by using different temporal and spatial grid sizes. The simulations show that the tearing mode is sensitive to thermal perturbations inside the island and less sensitive to thermal perturbations outside the island. The island grows larger when cooled inside the island interior and shrinks when heated inside the island. The simulations calculate different thermo-resistive tearing mode growths by increasing the plasma density. The results show that the maximum island width increases by a factor of 170% when the plasma density is increased from $0.8 n_G$ to $1.05 n_G$. The numerical model is also compared with the semi-analytical model by calculating the Δ' terms as defined in the modified Rutherford equations. Good agreement is observed between the two models.

Acknowledgments

Appendix. Convergence of simulations

As this work aims to study the tearing mode at the density limit, it is crucial to get converged island growth results. The convergence of the simulations are examined by varying the
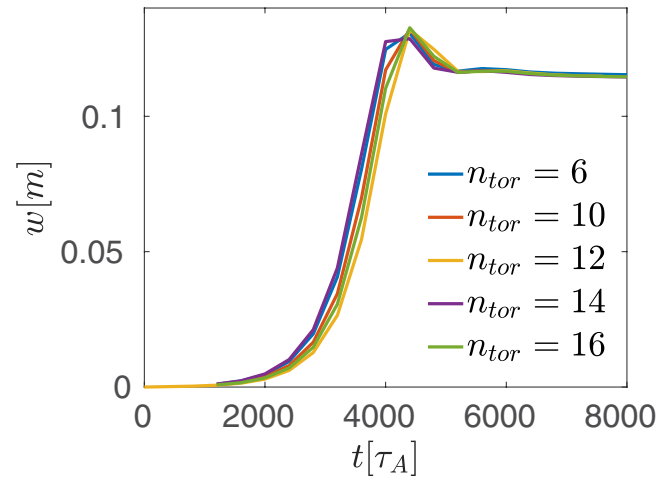

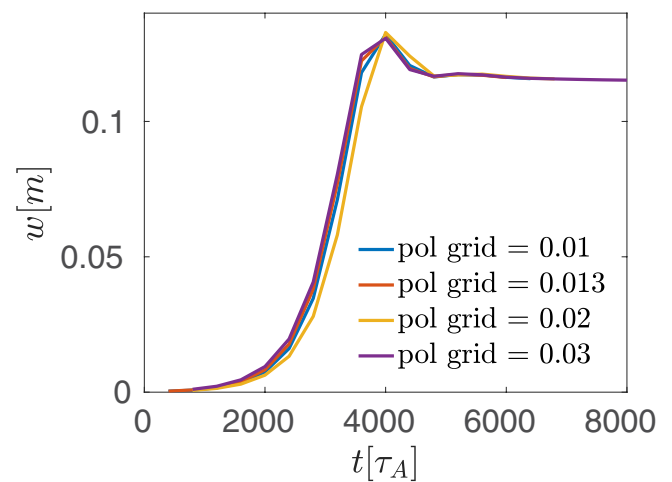**Figure A1.** The toroidal grid size convergence.

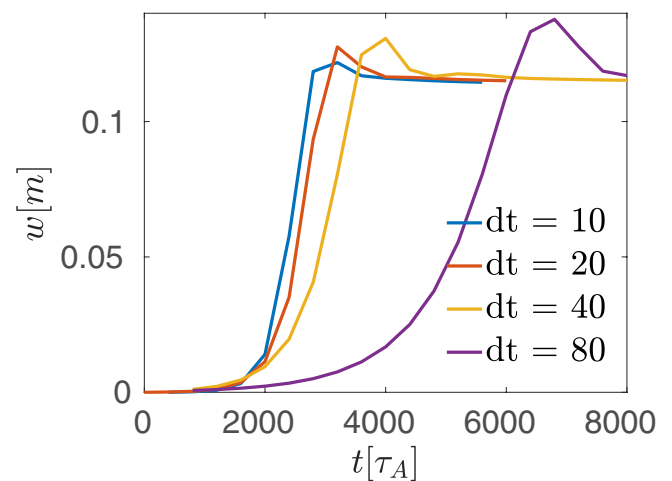**Figure A2.** The poloidal grid size convergence.

Figure A3. The time step size convergence.

toroidal grid size, the poloidal grid size and the time step size. In figure A1, the poloidal grid size is 0.03, the time step size is 40, and the number of toroidal planes is varied from 6 to 16. It is found that 6 toroidal planes is good enough to resolve the island growth. In figure A2, the number of toroidal planes is 6, the time step size is 40 and the poloidal grid size is varied

from 0.01 to 0.03. The island growth converges at the poloidal grid size of 0.03. In figure A3, the poloidal grid size is 0.03, the number of toroidal planes is 6, and the time step size is varied from 10 to 80. The island growth converges at the time step of 10. Therefore the tearing mode growth converges when the poloidal grid size is 0.03, the toroidal plane number is 6 and the time step size is 10.

References

[1] Teng Q., Brennan D., Delgado-Aparicio L., Gates D., Swerdlow J. and White R. 2016 A predictive model for the tokamak density limit *Nucl. Fusion* **56** 106001

[2] Jardin S.C., Ferraro N., Breslau J. and Chen J. 2012 Multiple timescale calculations of sawteeth and other global macroscopic dynamics of tokamak plasmas *Comput. Sci. Discovery* **5** 014002

[3] Artsimovich L. 1972 Tokamak devices *Nucl. Fusion* **12** 215

[4] Vershkov V. and Mirnov S. 1974 Role of impurities in current tokamak experiments *Nucl. Fusion* **14** 383

[5] Costa S., De Angelis R., Ortolani S. and Puiatti M. 1982 Total radiation measurements in the eta-beta ii experiment *Nucl. Fusion* **22** 1301

[6] Hugill J., Lomas P. and Wootton A. 1983 High density operation in dite with neutral beam injection *Technical Report* UKAEA Culham Lab

[7] Greenwald M., Terry J., Wolfe S., Ejima S., Bell M., Kaye S. and Neilson G. 1988 A new look at density limits in tokamaks *Nucl. Fusion* **28** 2199

[8] Greenwald M. 2002 Density limits in toroidal plasmas *Plasma Phys. Control. Fusion* **44** R27

[9] Furth H., Rosenbluth M., Rutherford P. and Stodiek W. 1970 Thermal equilibrium and stability of tokamak discharges *Phys. Fluids* **13** 3020–30

[10] Stangeby P.C. *et al* 2000 *The Plasma Boundary of Magnetic Fusion Devices* vol 224 (Bristol: Institute of Physics Publishing)

[11] Connor J. and You S. 2001 On the density limit in tokamaks *Plasma Phys. Control. Fusion* **44** 121

[12] Bombard B. 2015 Poloidal asymmetries in the limiter shadow plasma of the alcator c tokamak (https://dspace.mit.edu/bitstream/handle/1721.1/93554/86rr006_full.pdf?sequence=1)

[13] Lipschultz B. 1987 Review of marfe phenomena in tokamaks *J. Nucl. Mater.* **145** 15–25

[14] Valovic M. *et al* 2002 Long timescale density peaking in JET *Plasma Phys. Control. Fusion* **44** 1911

[15] Mahdavi M. *et al* 2002 High performance h mode plasmas at densities above the greenwald limit *Nucl. Fusion* **42** 52

[16] Kamada Y., Hosogane N., Yoshino R., Hirayama T. and Tsunematsu T. 1991 Study of the density limit with pellet fuelling in JT-60 *Nucl. Fusion* **31** 1827

[17] Lang P. *et al* 2012 High-density h-mode operation by pellet injection and elm mitigation with the new active in-vessel saddle coils in asdex upgrade *Nucl. Fusion* **52** 023017

[18] Suttrop W. *et al* 1997 Tearing mode formation and radiative edge cooling prior to density limit disruptions in asdex upgrade *Nucl. Fusion* **37** 119

[19] Jardin S.C., Breslau J. and Ferraro N. 2007 A high-order implicit finite element method for integrating the two-fluid magnetohydrodynamic equations in two dimensions *J. Comput. Phys.* **226** 2146–74

[20] Post D.E., Jensen R., Tarter C., Grasberger W. and Lokke W. 1977 Steady-state radiative cooling rates for low-density, high-temperature plasmas *At. Data Nucl. Data Tables* **20** 397–439

[21] White R.B., Monticello D.A., Rosenbluth M.N. and Waddell B.V. 1977 Saturation of the tearing mode *Phys. Fluids (1958–1988)* **20** 800–5

[22] White R.B., Gates D.A. and Brennan D.P. 2015 Thermal island destabilization and the greenwald limit *Phys. Plasmas* **22** 022514

[23] Zohm H. *et al* 1999 Experiments on neoclassical tearing mode stabilization by ECCD in ASDEX Upgrade *Nucl. Fusion* **39** 577

[24] Isayama A. *et al* 2000 Complete stabilization of a tearing mode in steady state high-βp h-mode discharges by the first harmonic electron cyclotron heating/current drive on JT-60u *Plasma Phys. Control. Fusion* **42** L37

[25] Westerhof E. *et al* 2007 Tearing mode stabilization by electron cyclotron resonance heating demonstrated in the textor tokamak and the implication for ITER *Nucl. Fusion* **47** 85

[26] Wesson J. *et al* 1989 Disruptions in JET *Nucl. Fusion* **29** 641

[27] Inagaki S. *et al* 2004 Observation of reduced heat transport inside the magnetic island o point in the large helical device *Phys. Rev. Lett.* **92** 055002

[28] Ida K., Kamiya K., Isayama A. and Sakamoto Y. 2012 Reduction of ion thermal diffusivity inside a magnetic island in JT-60u tokamak plasma *Phys. Rev. Lett.* **109** 065001